NEW DIFFRACTION DATA

Crystal structure of iprodione, $C_{13}H_{13}Cl_2N_3O_3$

James A. Kaduk[1,2], Anja Dosen[3] and Thomas N. Blanton[3]

[1]Department of Chemistry, Illinois Institute of Technology, 3101 South Dearborn Street, Chicago, IL 60616, USA
[2]Department of Physics, North Central College, 131 South Loomis Street, Naperville, IL 60540, USA
[3]International Centre for Diffraction Data (ICDD), 12 Campus Boulevard, Newtown Square, PA 19073-3273, USA

Abstract: The crystal structure of iprodione has been solved and refined using synchrotron X-ray powder diffraction data and optimized using density functional theory techniques. Iprodione crystallizes in the space group $P2_1/c$ (#14) with $a = 15.6469(3)$, $b = 22.8436(3)$, $c = 8.67226(10)$ Å, $\beta = 94.1303(7)°$, $V = 3,091.70(9)$ Å^3, and $Z = 8$ at 298 K. The crystal structure contains clusters of four iprodione molecules. The only two classical N–H⋯O hydrogen bonds in the structure are both intramolecular. The powder pattern has been submitted to the International Centre for Diffraction Data for inclusion in the Powder Diffraction File™ (PDF®).

I. INTRODUCTION

Iprodione (marketed under the trade name Rovral, among others) is a fungicide used for disease control in agricultural applications. Rovral can be applied to many food crops and ornamental plants. It functions by preventing the germination of fungal spores and inhibits the growth of fungal mycelium (PubChem; Kim et al., 2023). The systematic name (CAS Registry No. 36734-19-7) is 3-(3,5-dichlorophenyl)-2,4-dioxo-N-propan-2-ylimidazolidine-1-carboxamide. A two-dimensional molecular diagram of iprodione is shown in Figure 1. We are unaware of any experimental diffraction or structural data on this compound.

This work was carried out as part of a project (Kaduk et al., 2014) to determine the crystal structures of large-volume commercial pharmaceuticals and include high-quality powder diffraction data for them in the Powder Diffraction File™ (Kabekkodu et al., 2024).

II. EXPERIMENTAL

Iprodione was a commercial reagent, purchased from TargetMol (#T5116) and was used as received. The light yellow powder was packed into a 0.5-mm-diameter Kapton capillary and rotated during the measurement at ~2 Hz. The powder pattern was measured at 298(1) K at the Wiggler Low Energy Beamline (Leontowich et al., 2021) of the Brockhouse X-ray Diffraction and Scattering Sector of the Canadian Light Source using a wavelength of 0.819826(2) Å (15.1 keV) from 1.6 to 75.0° 2θ with a step size of 0.0025° and a collection time

of 3 minutes. The high-resolution powder diffraction data were collected using eight Dectris Mythen2 X series 1K linear strip detectors. NIST SRM 660b LaB$_6$ was used to calibrate the instrument and refine the monochromatic wavelength used in the experiment.

The pattern was indexed using JADE Pro (MDI, 2024) on a primitive monoclinic unit cell with $a = 15.65213$, $b = 22.84356$, $c = 8.67028$ Å, $\beta = 94.11°$, $V = 3,092.10$ Å^3, and $Z = 8$. The suggested space group was $P2_1/c$, which was confirmed by the successful solution and refinement of the structure. A reduced cell search of the Cambridge Structural Database (Groom et al., 2016) yielded 13 hits, but no structures for iprodione or its derivatives.

The iprodione molecular structure was downloaded from PubChem (Kim et al., 2023) as Conformer3D_COMPOUND_CID_37517.sdf. It was converted to a *.mol2 file using Mercury (Macrae et al., 2020). The crystal structure was solved using Monte Carlo-simulated annealing techniques as implemented in EXPO2014 (Altomare et al., 2013), using two molecules as fragments and a bump penalty.

Rietveld refinement was carried out with GSAS-II (Toby and Von Dreele, 2013). Only the 2.0–45.0° portion of the pattern was included in the refinements ($d_{min} = 1.071$ Å). All non-H-bond distances and angles were subjected to restraints, based on a Mercury/Mogul Geometry Check (Bruno et al., 2004; Sykes et al., 2011). The Mogul average and standard deviation for each quantity were used as the restraint parameters. The five- and six-membered rings in each molecule were restrained to be planar. The restraints contributed 3.2% to the overall χ^2. The hydrogen atoms were included in calculated positions, which were recalculated during the refinement using Materials Studio (Dassault

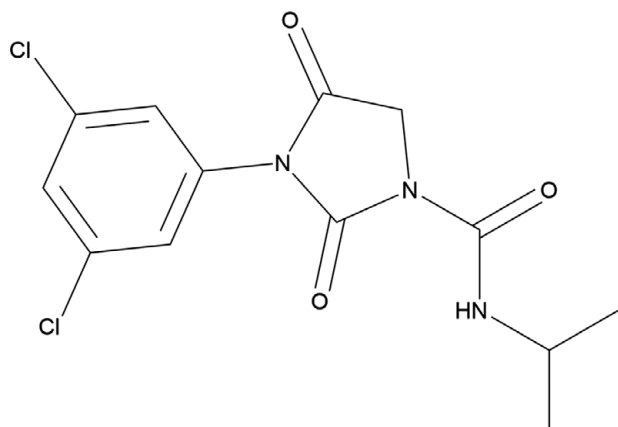Corresponding author: James A. Kaduk; Email: kaduk@polycrystallography.com

Figure 1. The two-dimensional structure of iprodione.

Systèmes, 2023). The U_{iso} of the heavy atoms were grouped by chemical similarity. The U_{iso} for the H atoms were fixed at 1.3× the U_{iso} of the heavy atoms to which they are attached. The peak profiles were described using the generalized (Stephens, 1999) microstrain model. The background was modeled using a three-term shifted Chebyshev polynomial, with peaks at 3.07 and 10.78° to model the narrow and broad scattering from the Kapton capillary and any amorphous component.

The final refinement of 160 variables using 17,201 observations and 112 restraints yielded the residual $R_{\text{wp}} = 0.05677$. The largest peak (1.35 Å from Cl36) and hole (1.10 Å from C12) in the difference Fourier map were 0.54(13) and −0.55 (13) $e\text{Å}^{-3}$, respectively. The final Rietveld plot is shown in Figure 2. The largest features in the normalized error plot are in the shapes of some of the strong low-angle peaks, and at

peaks of an unidentified inorganic crystalline impurity. These misfits probably indicate subtle changes in the specimen during the measurement.

The crystal structure of iprodione was optimized (fixed experimental unit cell) with density functional theory techniques using VASP (Kresse and Furthmüller, 1996) through the MedeA graphical interface (Materials Design, 2024). The calculation was carried out on 32 cores of a 144-core (768-GB memory) HPE Superdome Flex 280 Linux server at North Central College. The calculation used the GGA-PBE functional, a plane wave cutoff energy of 400.0 eV, and a k-point spacing of 0.5 Å^{-1}, leading to a $1 \times 1 \times 2$ mesh, and took ~25 hours. Single-point density functional calculations (fixed experimental cell) and population analysis were carried out using CRYSTAL23 (Erba et al., 2023). The basis sets for the H, C, N, and O atoms in the calculation were those of Gatti et al. (1994), and that for Cl was that of Peintinger et al. (2013). The calculations were run on a 3.5-GHz PC using eight k-points and the B3LYP functional and took ∼3.8 hours.

III. RESULTS AND DISCUSSION

There are two molecules in the asymmetric unit of iprodione. The root-mean-square (rms) Cartesian displacement of the non-H atoms in the Rietveld-refined and VASP-optimized structures of molecules 1 and 2 are 0.065 and 0.068 Å (Figures 3 and 4). The agreements are within the normal range for correct structures (van de Streek and Neumann, 2014). The two molecules differ in conformation (Figure 5); the rms displacement in the VASP-optimized structure is 1.187 Å and can be decreased to 0.246 Å by invoking the inversion option in Mercury. The contents of the asymmetric unit are illustrated in Figure 6. The
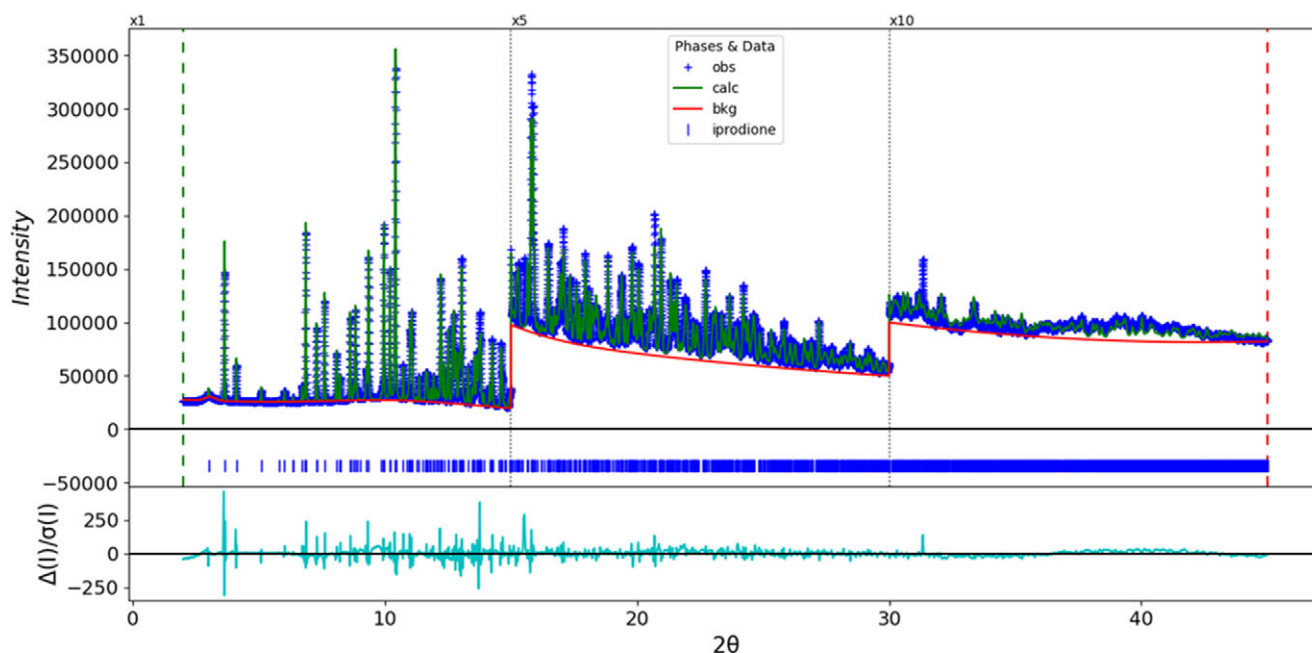

Figure 2. The Rietveld plot for iprodione. The blue crosses represent the observed data points, and the green line represents the calculated pattern. The cyan curve indicates the normalized error plot, and the red line indicates the background curve. The row of blue tick marks indicates the iprodione reflection positions. The vertical scale has been multiplied by a factor of 5× for 2θ > 15.0° and by a factor of 10× for 2θ > 30.0°.
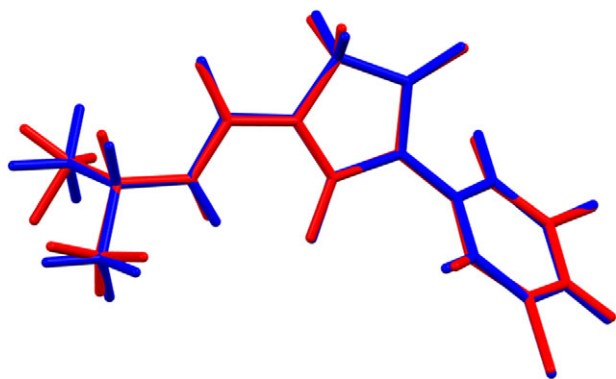
Figure 3. Comparison of the Rietveld-refined (red) and VASP-optimized (blue) structures of molecule 1 of iprodione. The root-mean-square Cartesian displacement is 0.065 Å. Image generated using Mercury (Macrae et al., 2020).
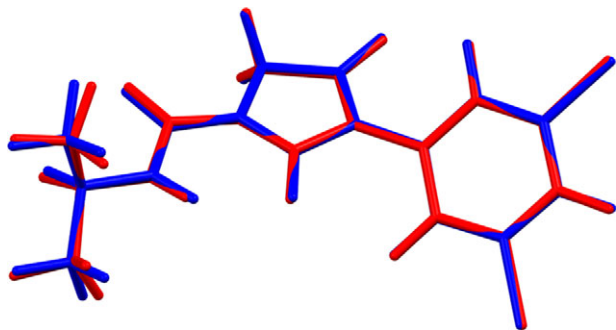

Figure 4. Comparison of the Rietveld-refined (red) and VASP-optimized (blue) structures of molecule 2 of iprodione. The root-mean-square Cartesian displacement is 0.068 Å. Image generated using Mercury (Macrae et al., 2020).
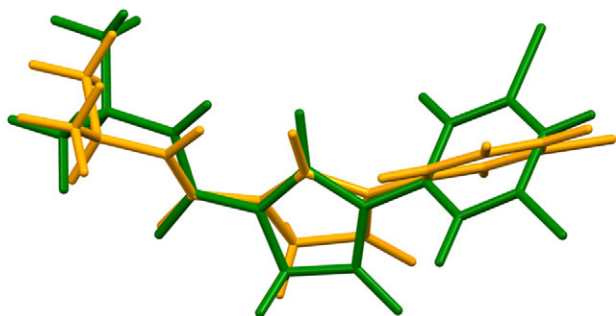

Figure 5. Comparison of molecule 1 (green) and molecule 2 (orange) in the VASP-optimized structure of iprodione. The root-mean-square Cartesian displacement is 1.187 Å. Image generated using Mercury (Macrae et al., 2020).

remaining discussion will emphasize the VASP-optimized structure.

All of the bond distances and bond angles and almost all the torsion angles fall within the normal ranges indicated by a Mercury Mogul Geometry check (Macrae et al., 2020). Only the N42–C47–N40–C44 torsion angle of −23.2° is flagged as unusual. This lies on the tail of a narrow distribution of similar
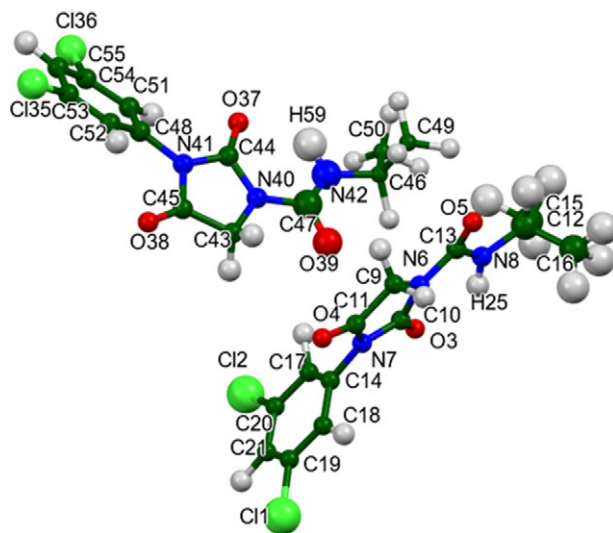

Figure 6. The asymmetric unit of iprodione, with the atom numbering. The atoms are represented by 50% probability spheroids. Image generated using Mercury (Macrae et al., 2020).

torsion angles around 0°. The conformation of molecule 2 is slightly unusual.

Quantum chemical geometry optimization of an isolated iprodione molecule (DFT/B3LYP/6-31G*/water) using Spartan '24 (Wavefunction, 2023) indicated that the two independent molecules are within 0.03 kcal/mol of each other in energy. Each is close to the global minimum-energy conformation, which has a slightly different orientation of the dichlorophenyl group.

The crystal structure (Figure 7) contains clusters of four iprodione molecules. The Mercury Aromatics Analyser indicates one moderate interaction, with a minimum ring–ring distance between the independent molecules of 5.48 Å. Despite the visual appearance, fingerprint plots indicate that only 1.3% of the intermolecular contacts are Cl···Cl.

Analysis of the contributions to the total crystal energy of the structure using the Forcite module of Materials Studio (Dassault Systèmes, 2023) indicates that the intramolecular energy is dominated by angle distortion terms. The intermolecular energy is dominated by electrostatic attractions, which in this force field-based analysis also includes hydrogen bonds. The hydrogen bonds are better discussed using the results of the DFT calculation.

There are only two classical hydrogen bonds in the structure, and they are both intramolecular N–H···O hydrogen bonds (Table I). The energies of the N–H···O hydrogen bonds were calculated using the correlation of Wheatley and Kaduk (2019). Several C–H···O and one C–H···Cl hydrogen bonds also contribute to the lattice energy.

The volume enclosed by the Hirshfeld surface of iprodione (Figure 8; Hirshfeld, 1977; Spackman et al., 2021) is 762.77 Å^3, 98.69% of one-fourth of the unit cell volume. The packing density is thus typical. The only significant close contacts (red in Figure 8) involve the hydrogen bonds. The volume/non-hydrogen atom is normal at 18.4 Å^3.

The Bravais–Friedel–Donnay–Harker (Bravais, 1866; Friedel, 1907; Donnay and Harker, 1937) algorithm suggests
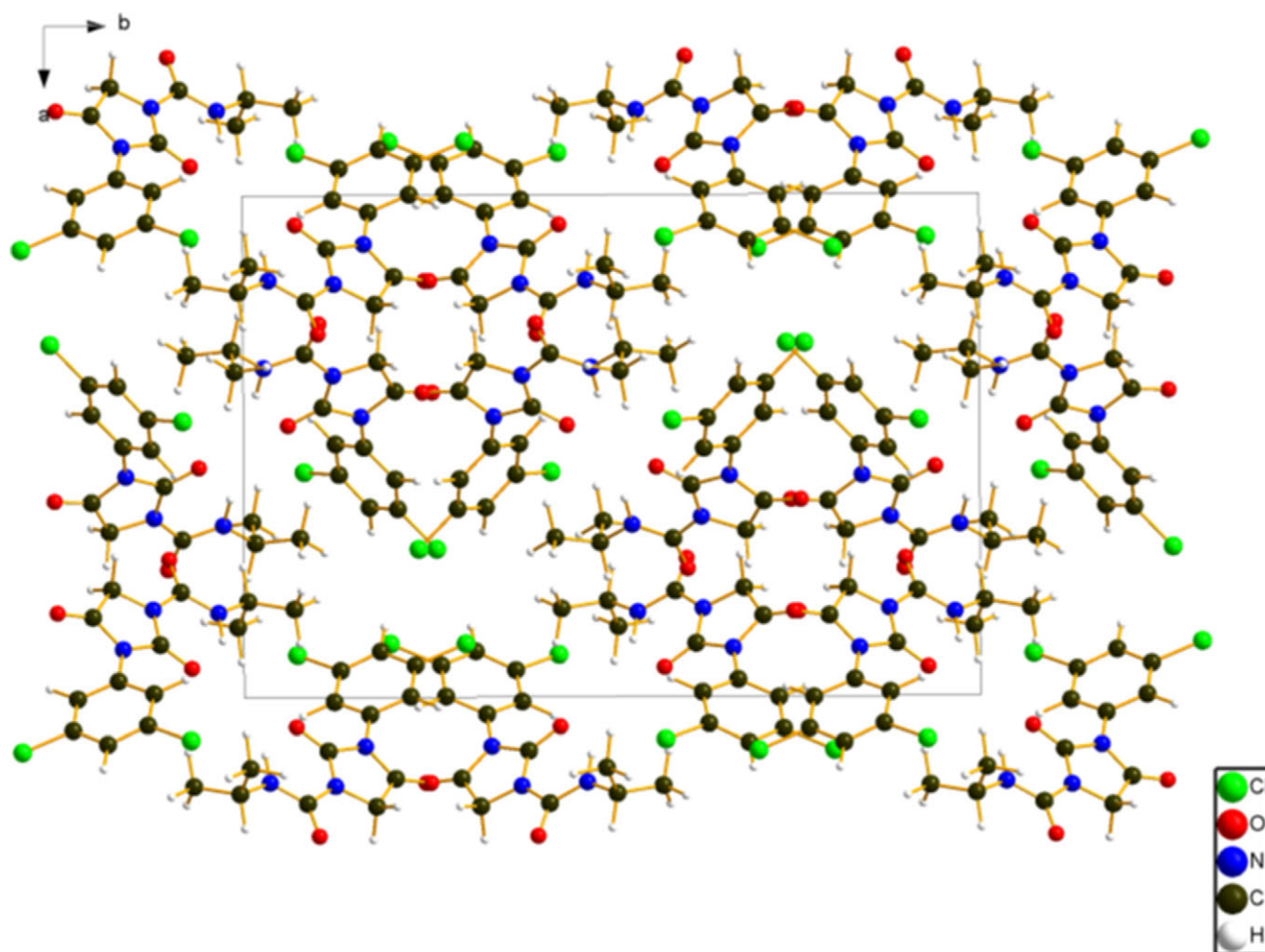
Figure 7. The crystal structure of iprodione, viewed down the *c*-axis. Image generated using Diamond (Crystal Impact, 2023).

TABLE I. Hydrogen bonds (CRYSTAL23) in iprodione

H bond	D–H, Å	H···A, Å	D···A, Å	D–H···A, °	Mulliken overlap, *e*	*E*, kcal/mol
N42–H59···O37	1.026	1.928[a]	2.753	132.2	0.044	4.8
N8–H25···O3	1.026	1.944[a]	2.694	126.3	0.041	4.7
C52–H67···O38	1.086	2.401[a]	2.872	106.4	0.012	
C50–H64···O37	1.100	2.685	3.698	152.9	0.010	
C46–H58···O39	1.101	2.461	2.861	99.7	0.011	
C43–H57···O4	1.100	2.516	3.299	133.8	0.016	
C43–H56···O38	1.100	2.173	3.299	159.9	0.025	
C21–H34···Cl1	1.088	2.861	3.789	144.2	0.014	
C15–H27···O3	1.099	2.530	3.521	149.5	0.011	
C12–H24···O5	1.101	2.513	2.849	96.1	0.011	
C9–H23···O4	1.101	2.239	3.316	173.6	0.024	
C9–H22···O38	1.101	2.480	3.464	137.1	0.019	

[a]Intramolecular.

that we might expect elongated morphology for iprodione, with [001] as the long axis. A second-order spherical harmonic model was included in the refinement. The texture index was 1.006(0), indicating that the preferred orientation was not significant in this rotated capillary specimen.

DEPOSITED DATA

The powder pattern of iprodione from this synchrotron dataset has been submitted to the International Centre for Diffraction Data (ICDD) for inclusion in the Powder Diffraction File. The Crystallographic Information Framework (CIF)
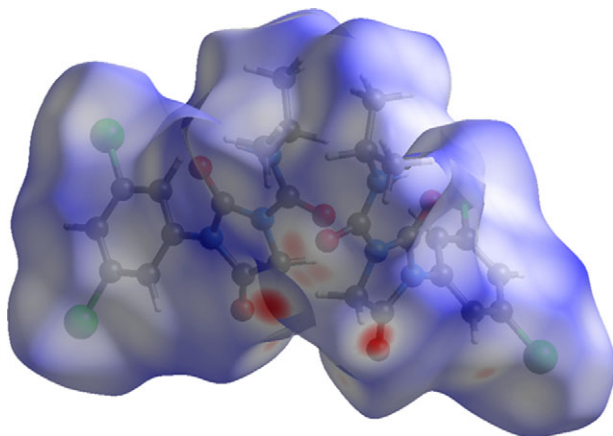
Figure 8. The Hirshfeld surface of iprodione. The intermolecular contacts longer than the sums of the van der Waals radii are colored blue, and the contacts shorter than the sums of the radii are colored red. The contacts equal to the sums of radii are white. Image generated using CrystalExplorer (Spackman et al., 2021).

files containing the results of the Rietveld refinement (including the raw data) and the DFT geometry optimization were deposited with the ICDD. The data can be requested at pdj@icdd.com.

CONFLICTS OF INTEREST

The authors have no conflicts of interest to declare.

REFERENCES

Altomare, A., C. Cuocci, C. Giacovazzo, A. Moliterni, R. Rizzi, N. Corriero, and A. Falcicchio. 2013. "EXPO2013: A Kit of Tools for Phasing Crystal Structures from Powder Data." *Journal of Applied Crystallography* 46: 1231–35.

Bravais, A. 1866. *Etudes Cristallographiques*. Gauthier Villars.

Bruno, I. J., J. C. Cole, M. Kessler, J. Luo, W. D. S. Motherwell, L. H. Purkis, B. R. Smith, et al. 2004. "Retrieval of Crystallographically Derived Molecular Geometry Information." *Journal of Chemical Information and Computer Sciences* 44: 2133–44.

Crystal Impact. 2023. *Diamond V. 5.0.0*. Crystal Impact – Dr. H. Putz & Dr. K. Brandenburg.

Dassault Systèmes. 2023. *BIOVIA Materials Studio 2024*. BIOVIA.

Donnay, J. D. H., and D. Harker. 1937. "A New Law of Crystal Morphology Extending the Law of Bravais." *American Mineralogist* 22: 446–67.

Erba, A., J. K. Desmarais, S. Casassa, B. Civalleri, L. Donà, I. J. Bush, B. Searle, et al. 2023. "CRYSTAL23: A Program for Computational Solid State Physics and Chemistry." *Journal of Chemical Theory and Computation* 19: 6891–932. https://doi.org/10.1021/acs.jctc.2c00958.

Friedel, G. 1907. "Etudes sur la loi de Bravais." *Bulletin de la Société Française de Minéralogie* 30: 326–455.

Gatti, C., V. R. Saunders, and C. Roetti. 1994. "Crystal-Field Effects on the Topological Properties of the Electron-Density in Molecular Crystals – the Case of Urea." *Journal of Chemical Physics* 101: 10686–96.

Groom, C. R., I. J. Bruno, M. P. Lightfoot, and S. C. Ward. 2016. "The Cambridge Structural Database." *Acta Crystallographica Section B: Structural Science, Crystal Engineering and Materials* 72: 171–79.

Hirshfeld, F. L. 1977. "Bonded-Atom Fragments for Describing Molecular Charge Densities." *Theoretica Chemica Acta* 44: 129–38.

Kabekkodu, S., A. Dosen, and T. N. Blanton. 2024. "PDF-5+: A Comprehensive Powder Diffraction File™ for Materials Characterization." *Powder Diffraction* 39: 47–59.

Kaduk, J. A., C. E. Crowder, K. Zhong, T. G. Fawcett, and M. R. Suchomel. 2014. "Crystal Structure of Atomoxetine Hydrochloride (Strattera), $C_{17}H_{22}NOCl$." *Powder Diffraction* 29: 269–73.

Kim S., J. Chen, T. Cheng, A. Gindulyte, J. He, S. He, Q. Li, et al. 2023. "PubChem 2023 Update." *Nucleic Acids Research* 51 (D1):D1373–80. https://doi.org/10.1093/nar/gkac956.

Kresse, G., and J. Furthmüller. 1996. "Efficiency of Ab-Initio Total Energy Calculations for Metals and Semiconductors Using a Plane-Wave Basis Set." *Computational Materials Science* 6: 15–50.

Leontowich, A. F. G., A. Gomez, B. Diaz Moreno, D. Muir, D. Spasyuk, G. King, J. W. Reid, C.-Y. Kim, and S. Kycia. 2021. "The Lower Energy Diffraction and Scattering Side-Bounce Beamline for Materials Science at the Canadian Light Source." *Journal of Synchrotron Radiation* 28: 1–9. https://doi.org/10.1107/S1600577521002496.

Macrae, C. F., I. Sovago, S. J. Cottrell, P. T. A. Galek, P. McCabe, E. Pidcock, M. Platings, et al. 2020. "*Mercury 4.0*: From Visualization to Design and Prediction." *Journal of Applied Crystallography* 53: 226–35.

Materials Design. 2024. *MedeA 3.7.2*. Materials Design, Inc.

MDI. 2024. *JADE Pro Version 9.0*. Materials Data.

Peintinger, M. F., D. Vilela Oliveira, and T. Bredow. 2013. "Consistent Gaussian Basis Sets of Triple-Zeta Valence with Polarization Quality for Solid-State Calculations." *Journal of Computational Chemistry* 34: 451–59.

Spackman, P. R., M. J. Turner, J. J. McKinnon, S. K. Wolff, D. J. Grimwood, D. Jayatilaka, and M. A. Spackman. 2021. "CrystalExplorer: A Program for Hirshfeld Surface Analysis, Visualization and Quantitative Analysis of Molecular Crystals." *Journal of Applied Crystallography* 54: 1006–11. https://doi.org/10.1107/S1600576721002910; https://crystalexplorer.net.

Stephens, P. W. 1999. "Phenomenological Model of Anisotropic Peak Broadening in Powder Diffraction." *Journal of Applied Crystallography* 32: 281–89.

Sykes, R. A., P. McCabe, F. H. Allen, G. M. Battle, I. J. Bruno, and P. A. Wood. 2011. "New Software for Statistical Analysis of Cambridge Structural Database Data." *Journal of Applied Crystallography* 44: 882–86.

Toby, B. H., and R. B. Von Dreele. 2013. "GSAS II: The Genesis of a Modern Open Source All Purpose Crystallography Software Package." *Journal of Applied Crystallography* 46: 544–49.

van de Streek, J., and M. A. Neumann. 2014. "Validation of Molecular Crystal Structures from Powder Diffraction Data with Dispersion-Corrected Density Functional Theory (DFT-D)." *Acta Crystallographica Section B: Structural Science, Crystal Engineering and Materials* 70: 1020–32.

Wavefunction, Inc. 2023. *Spartan '24. V. 1.0.0. Placeholder Text*Placeholder Text Wavefunction, Inc.

Wheatley, A. M., and J. A. Kaduk. 2019. "Crystal Structures of Ammonium Citrates." *Powder Diffraction* 34: 35–43.